

RESEARCH

Open Access



# Assessing intra- and interfraction motion and its dosimetric impacts on cervical cancer adaptive radiotherapy based on 1.5T MR-Linac

Huadong Wang<sup>1</sup>, Zhenkai Li<sup>1,3</sup>, Dengxin Shi<sup>1</sup>, Peijun Yin<sup>1</sup>, Benzhe Liang<sup>1,4</sup>, Jingmin Zou<sup>1,2</sup>, Qiuqing Tao<sup>1,5</sup>, Wencheng Ma<sup>1,2</sup>, Yong Yin<sup>1\*</sup> and Zhenjiang Li<sup>1\*</sup>

## Abstract

**Purpose** The purpose of this study was to quantify the intra- and interfraction motion of the target volume and organs at risk (OARs) during adaptive radiotherapy (ART) for uterine cervical cancer (UCC) using MR-Linac and to identify appropriate UCC target volume margins for adapt-to-shape (ATS) and adapt-to-position (ATP) workflows. Then, the dosimetric differences caused by motion were analyzed.

**Methods** Thirty-two UCC patients were included. Magnetic resonance (MR) images were obtained before and after each treatment. The maximum and average shifts in the centroid of the target volume and OARs along the anterior/posterior (A/P: Y axes), cranial/caudal (Cr/C: Z axes), and right/left (R/L: X axes) directions were analyzed through image contours. The bladder wall deformation in six directions and the differences in the volume of the organs were also analyzed. Additionally, the motion of the upper, middle and lower rectum was quantified. The correlation between OAR displacement/deformation and target volume displacement was evaluated. The planning CT dose distribution was mapped to the MR image to generate a plan based on the new anatomy, and the dosimetric differences caused by motion were analyzed.

**Results** For intrafraction motion, the clinical tumor volume (CTV) range of motion along the XYZ axes was within 5 mm; for interfraction motion, the range of motion along the X axis was within 5 mm, and the maximum distances of motion along the Y axis and Z axis were 7.45 and 6.59 mm, respectively. Additionally, deformation of the superior and anterior walls of the bladder was most noticeable. The largest magnitude of motion was observed in the upper segment of the rectum. Posterior bladder wall displacement was correlated with rectal and CTV centroid Y-axis displacement ( $r=0.63$ ,  $r=0.50$ ,  $P<0.05$ ). Compared with the interfractional plan, a significant decrease in the planning target volume (PTV) D98 (7.5 Gy, 7.54 Gy) was observed. However, there were no significant differences within the intrafraction.

**Conclusion** During ART for UCC patients using MR-Linac, we recommend an ATS workflow using isotropic PTV margins of 5 mm based on intrafraction motion. Based on interfraction motion, the recommended ATP workflow uses

\*Correspondence:

Yong Yin  
yinyongsd@126.com  
Zhenjiang Li  
zhenjli1987@163.com

Full list of author information is available at the end of the article



© The Author(s) 2024. **Open Access** This article is licensed under a Creative Commons Attribution-NonCommercial-NoDerivatives 4.0 International License, which permits any non-commercial use, sharing, distribution and reproduction in any medium or format, as long as you give appropriate credit to the original author(s) and the source, provide a link to the Creative Commons licence, and indicate if you modified the licensed material. You do not have permission under this licence to share adapted material derived from this article or parts of it. The images or other third party material in this article are included in the article's Creative Commons licence, unless indicated otherwise in a credit line to the material. If material is not included in the article's Creative Commons licence and your intended use is not permitted by statutory regulation or exceeds the permitted use, you will need to obtain permission directly from the copyright holder. To view a copy of this licence, visit <http://creativecommons.org/licenses/by-nc-nd/4.0/>.

anisotropic PTV margins of 5 mm in the R/L direction, 8 mm in the A/P direction, and 7 mm in the Cr/C direction to compensate for dosimetric errors due to motion.

**Keywords** MR-Linac, Cervical cancer, Adaptive radiotherapy, Intra- and interfraction motion, Dosimetric difference

## Introduction

Uterine cervical cancer (UCC) is a common malignancy among women, with a global incidence of 7%, ranking fourth among all malignancies, and a mortality rate of 4%, ranking sixth [1, 2]. For locally advanced UCC, the standard treatment includes external beam radiotherapy (EBRT) combined with chemotherapy, followed by brachytherapy [3]. Thus, EBRT plays a crucial role in the treatment of locally advanced UCC, where intensity-modulated radiotherapy (IMRT) offers higher dose gradients, a more uniform dose distribution, and a reduced radiation dose to critical organs [4, 5]. Additionally, to minimize late toxicity to organs at risk (OARs), such as the bladder, rectum, and small intestine, highly precise treatment plans using IMRT have become the standard for providing safe and effective radiation therapy [6].

Patients with UCC can exhibit large changes in anatomy, potentially reducing the efficacy of treatment or increasing the dose to healthy OARs [7]. In clinical practice, cone-beam computed tomography (CBCT) is commonly used for guiding IMRT to compensate for the resulting dosimetric errors [8–10]. However, CBCT has many limitations. First, although the bladder can be clearly displayed, the boundary between the target volume and other tissues is not clear, making it difficult to delineate. Second, there is radiation exposure during scanning, so the number of scans should be minimized to avoid unnecessary radiation doses [11]. Third, compared to planning CT, CBCT has inaccurate Hounsfield units (HUs) [12]. When adapting treatment plans online, it is often necessary to convert CBCT images to synthetic CT (sCT) images to improve the accuracy of the electron density values to ensure accurate dose calculations [13]. Common methods include generating sCT images based on deep learning networks [14–16]. This invariably adds to the complexity of online adaptive radiotherapy. Therefore, it is difficult to make real-time adjustments to treatment plans using CBCT images after identifying the motion of the target area and OARs.

Compared to CBCT-guided conventional linear accelerators, the Unity MR-Linac (Elekta AB, Stockholm, Sweden) is superior. First, MR images have superior soft-tissue contrast, which is a significant advantage for delineating anatomical structures in the abdominopelvic region [17, 18]. Second, continuous MRI scans can be performed during irradiation and treatment rack rotation, and the scans do not produce additional exposure to ionizing radiation [19]. In addition, real-time 2D cine imaging enables visualization of the contours

of the region of interest (ROI), with three orthogonal planes centered on the tumor displayed simultaneously [19]. Moreover, Unity enables gated radiotherapy based on tumor location, with the dose delivered only when the tumor is located within the gating window [18]. As a result, MRI-guided radiotherapy (MRgRT) minimizes errors in interfraction setup and potentially allows for intrafraction motion correction using continuous MRI acquisition, thereby reducing the planning target volume (PTV) margins used to ensure target dose delivery [17, 20]. Unity integrates a 7 MV linear accelerator and a 1.5 T diagnostic MRI scanner [21, 22] and provides both adapt-to-shape (ATS) and adapt-to-position (ATP) workflows [23]. For the ATS workflow, the ROI must be re-delineated for each treatment to adapt to online anatomical changes. Therefore, the determination of the PTV margins for the ATS plan only needs to consider intrafraction movement. However, MR images have no electron density information and cannot be used for calculating the planned dose. Unity mainly solves this problem by generating sCT images based on the electron density information of the planning CT by assigning the mean electron density to the ROIs of MR images [24]. The ATP workflow is only required to register the reference CT and online MR images, correct the isocenter locations, and reoptimize the plan. Therefore, the PTV margins of the ATP plan also need to consider interfraction motion. In summary, the anatomical structure of UCC patients changes considerably during treatment [25, 26]. Appropriate PTV margins must be selected for the ATS and ATP workflows based on intra- and interfraction motion, respectively.

Although MRgRT allows for precise organ delineation, bladder filling and rectal peristalsis during EBRT for patients with UCC can result in continuous organ deformation and displacement, affecting the displacement and deformation of the target volume and thus compromising dose accuracy [27–29]. However, specific dosimetric loss caused by intra- and interfraction motion is not known in adaptive radiotherapy for cervical cancer using 1.5T MR-Linac [30].

Based on the above findings, we designed an MR-Linac-guided radiation therapy protocol for UCC patients. The aims of this study were as follows: (1) to quantify the intra- and interfractional volume and positional changes in the target volume to identify appropriate PTV margins for ATP and ATS workflows; (2) to quantify the volume and positional changes in the bladder and rectum and analyze the correlation between OAR changes and the

target volume motion; and (3) to analyze the dosimetric differences caused by intra- and interfraction motion.

## Materials and methods

### Patient information

This study included 32 UCC patients who received adaptive radiotherapy at Shandong Cancer Hospital between 2021 and 2022. The treatment involved a combination of IMRT and brachytherapy, with brachytherapy performed in the last 1–2 weeks of IMRT. The IMRT target area received a reference dose of 46–50 Gy (2 Gy  $\times$  23/25 fractions), and the overall treatment duration was 4–5 weeks. IMRT was conducted with patients in the supine position using a 1.5T MR-Linac system (Elekta Unity). Detailed information can be found in Table 1.

### Image acquisition

The treatment process included 4 image scans: CT simulation, 3.0T MR simulation, and pre- and posttreatment 1.5T MR scans (see Fig. 1). CT simulation began with patients drinking 500 ml of water one hour prior to scanning to achieve a consistent bladder volume. Prior to each treatment, a 1.5T MR scan with the same bladder filling strategy was performed. To shorten the online treatment time, images were acquired again two minutes before the end of treatment, which we defined as posttreatment 1.5T MRI. The time between pre- and posttreatment MR images was considered the treatment time. The Unity pelvic MR scan parameters were as follows: scan time=2 min, ACQ matrix=268 $\times$ 267, FOV=400 $\times$ 400 mm, TR=1532 ms, and TE=278 ms. Overall treatment lasted 4–5 weeks with weekly MR acquisitions. Each patient had 10 sets of MR images (5 pre- and 5 posttreatment), totaling 320 sets (160 pre- and 160 posttreatment). Unity acquires 1.5T MR images primarily for the validation and correction of treatment

locations and to observe changes in target volume during treatment, with no simulation role. The 3.0T MR simulation scan parameters were as follows: T1-weighted images (TR=4.5 ms, TE=2.0 ms, flip angle=15°), T2-weighted images (TR=7,059 ms, TE=75 ms, flip angle=110°) and T1-weighted enhanced images.

### Image delineation

The clinical tumor volume (CTV) included the gross tumor volume (GTV), uterus, cervix, parametrial tissue, upper 1/3 of the vagina, and regional lymph nodes (common iliac, external iliac, obturator, and presacral). The PTV was generated by adding a 5 mm isotropic margin to the CTV. The rectum was delineated from the anus (ischial tuberosity level) to the rectum–sigmoid colon junction. The bladder was delineated by outlining the filled bladder wall. The above work was performed by two experienced radiation oncologists who followed the Federation International of Gynecology and Obstetrics (RTOG) contouring guidelines for UCC [32] using semi-automated deformation delineation in conjunction with manual modifications.

### Plan design

Using Unity MR-Linac TPS Monaco (v5.40.04) and the GPU-based Monte Carlo dose calculation platform (GPUMCD), reference plans were created for 32 patients based on CT images. Nine-field IMRT plans were generated by adhering to the prescribed dose requirements: >95% target volume coverage and a maximum dose  $\leq$  110% of the prescribed dose. The OAR dose limit followed the International Commission on Radiation Units and Measurements (ICRU) Report No. 83 guidelines (see Supplementary Table 1).

### Organ motion analysis

The deformation and displacement of the image contours were analyzed using MIM software (MIM Maestro, version 7.1.9, Maastricht, Belgium). For interfraction motion, MR images (pre- and posttreatment) were compared with CT reference images; for intrafraction motion, posttreatment MR images were compared with pretreatment MR reference images. For each patient, 1.5T MR images were rigidly registered to the reference images based on bony structures. The contours of the target volume and OARs were mapped to the reference images (CT and posttreatment MRI). As shown in Fig. 2 (a), the displacements of the centroids of the target volume and OARs in the left–right (X axis), anterior–posterior (Y axis), and cranial–caudal (Z axis) directions were calculated.

For the bladder, as shown in Fig. 2 (b), the wall shift distance ( $\Delta d$ ) =  $OA_1 - OA_2$ . Additionally, by analyzing the pre- and posttreatment bladder volumes and treatment

**Table 1** Patient characteristics

	Values
Years	median: 52 range: 33–74
Staging	
IB	7 (22.0%)
II	5 (16.0%)
III	1 (3.0%)
IIIB	2 (6.0%)
IIIC	14 (44.0%)
IVB	1 (3.0%)
stage unknown	2 (6.0%)
Pathological classification	
squamous cell carcinoma	23 (72.0%)
adenocarcinoma	7 (22.0%)
mixed carcinoma	2 (6.0%)

IMRT: Intensity-modulated radiotherapy. UCC staging followed the criteria established by the Federation International of Gynecology and Obstetrics (FIGO) [31]

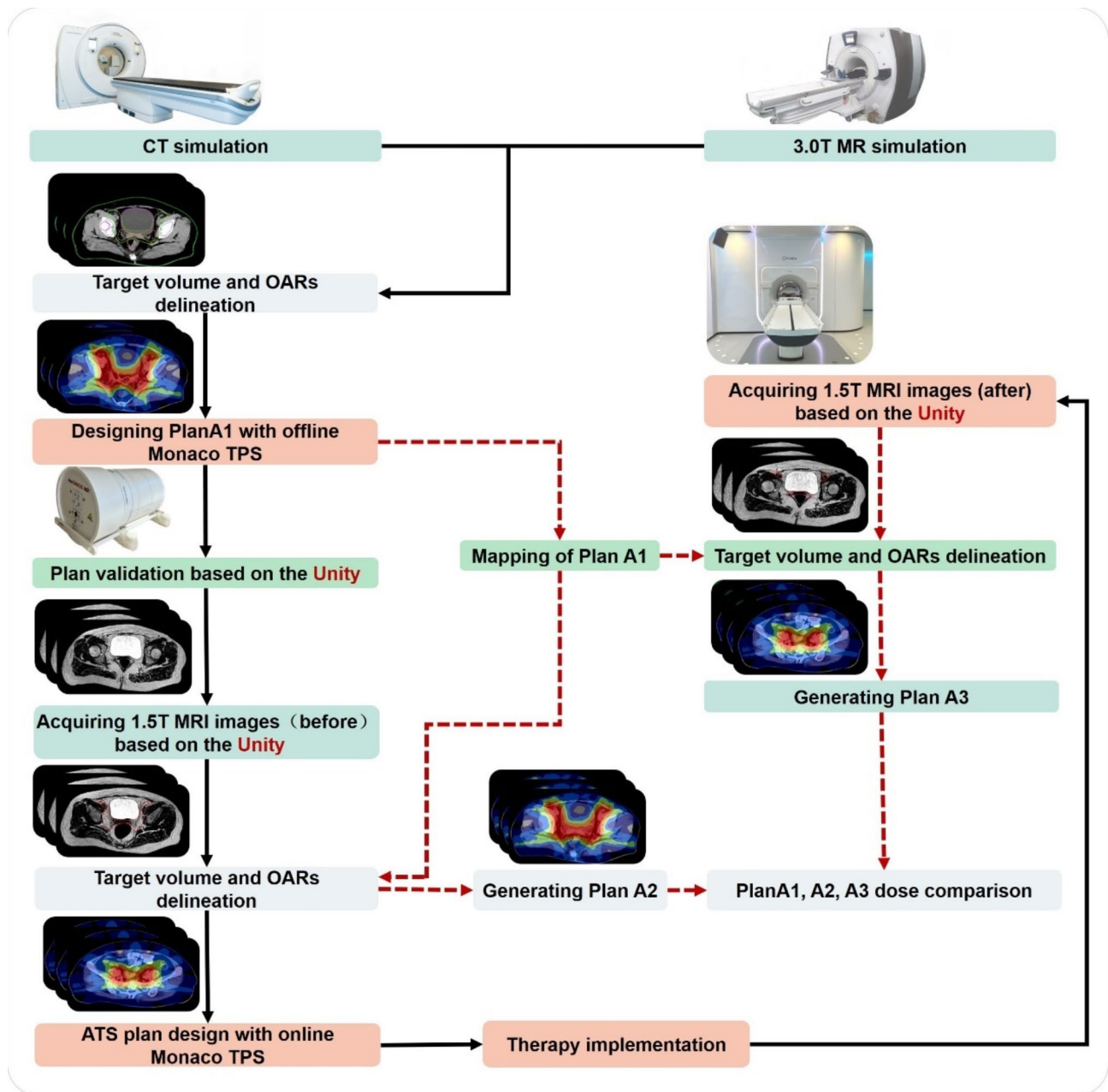


**Fig. 1** Patient treatment and experimental design flowchart. The entire treatment process is connected by solid black lines, while the process of dose mapping is connected by dashed red lines. OARs, organs at risk; ATS, adapt to shape; and Monaco TPS, Monaco Treatment Planning System. 1.5T MR-Linac is also known simply as Unity

time, the interfractional changes and filling rate can be determined. The rectum, which is a long tubular structure with different ranges of motion in the superior–inferior direction, was divided into three equal parts (upper, middle, and lower) for separate motion analysis. The correlations between the centroid displacement of the PTV and CTV and the bladder volume change, bladder wall deformation, and bladder–rectum centroid displacement were analyzed.

The DICE coefficient was used to assess the spatial overlap of organ and target volumes between pre- and posttreatment. The DICE coefficient is defined as  $2 * (A \cap B) / (A + B)$ , where A and B represent the volumes of the organ and target, respectively.

**Dose comparison**

In Fig. 1, planCT and 1.5T MR images were fused and registered. The planA dose was then mapped onto the structural contours of 1.5T MR (pre- and post-MRI)

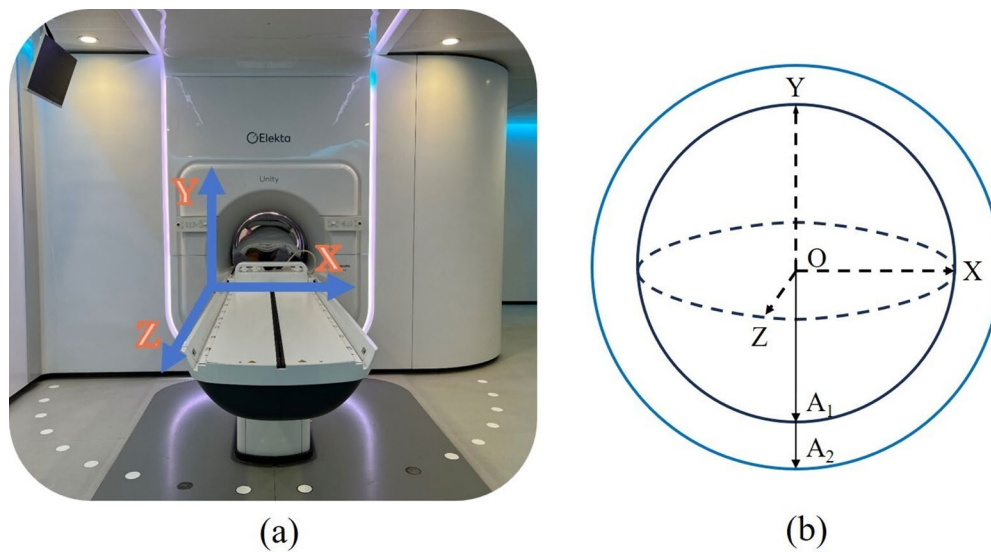


**Fig. 2** Coordinate system of motion. X axis (left–right), Y axis (anterior–posterior), and Z axis (cranial–caudal). O represents the centroid of the bladder contour in the reference image;  $OA_1$  (reference image) and  $OA_2$  (1.5T MR image) represent the distances from the centroid to the bladder apex

to create planA1 and planA2. These plans were compared based on their doses. The dose–volume histogram (DVH) parameters include the PTV, D1 cc, D2, D50, and D98, where Dx represents the dose received by X% of the target volume, maximum dose (Dmax), mean dose (Dmean), minimum dose (Dmin), heterogeneity index (HI), and conformity index (CI); for the bladder and rectum volume, the parameters include V10–V50 (Vx represents the volume percentage receiving more than X Gy), Dmean, Dmax, and Dmin; and for the spinal cord, the parameters include Dmean, Dmax, and Dmin.

### Statistical analysis

OriginPro2021 was used for the statistical analysis. Continuous data are presented as the mean  $\pm$  standard deviation (SD). To compare the two sets of data, a normality test was conducted. If the data were normally distributed, a paired t test was used. Otherwise, a Wilcoxon signed-rank test was employed. For the comparison of Plan A, A1, and A2, a normality test was performed. If the data followed a normal distribution, one-way ANOVA was used. Otherwise, Kruskal–Wallis ANOVA was employed.

The Pearson correlation coefficient was used to analyze the correlation between the changes in bladder volume, bladder wall displacement, bladder centroid, rectum centroid, PTV centroid displacement, and CTV centroid displacement. A correlation coefficient  $|r| < 0.4$  indicated a weak correlation, 0.4–0.7 indicated a moderate correlation, and  $>0.7$  indicated a strong correlation. The significance level for the tests was  $\alpha=0.05$ .

**Table 2** Displacement of the bladder wall and volume change

Intrafraction		
Volume	$\Delta d$ (MR post-pre) (ml)	$\Delta d/\Delta t$ (ml/min)
	$85.68 \pm 70.32$	$3.13 \pm 2.42$
Bladder wall	$\Delta x$ (MR post-pre) (mm)	$\Delta x/\Delta t$ (ml/min)
Superior	$9.30 \pm 8.77$	$0.34 \pm 0.32$
Inferior	$0.73 \pm 1.67$	$0.06 \pm 0.22$
Anterior	$3.28 \pm 4.89$	$0.12 \pm 0.18$
Posterior	$2.66 \pm 4.44$	$0.10 \pm 0.16$
Right	$1.53 \pm 2.38$	$0.06 \pm 0.09$
Left	$1.62 \pm 2.57$	$0.06 \pm 0.09$
Interfraction		
Volume	$\Delta d$ (CT-MRpre) (ml)	$\Delta d$ (CT-MRpost) (ml)
	106.23	20.3
Bladder wall	$\Delta x$ (CT-MRpre) (mm)	$\Delta x$ (CT-MRpost) (mm)
Superior	$5.71 \pm 23.86$	$-3.14 \pm 23.60$
Inferior	$0.71 \pm 3.67$	$-0.32 \pm 3.54$
Anterior	$9.04 \pm 11.13$	$5.87 \pm 12.33$
Posterior	$2.04 \pm 8.35$	$-0.24 \pm 8.52$
Right	$2.87 \pm 5.23$	$1.91 \pm 5.13$
Left	$3.05 \pm 4.85$	$1.09 \pm 4.79$

## Results

### Deformation and displacement of the bladder wall

#### Intrafraction

The mean treatment time ( $\Delta t$ ) was 27.5 (6.6) minutes. As shown in Table 2, the average increase in bladder volume was 85.68 (70.32) ml, with an average filling rate of 3.13 (2.42) ml/min. The greatest bladder wall displacement was in the superior wall ( $9.30 \pm 8.77$  mm), followed by the anterior wall ( $3.28 \pm 4.89$  mm), and the smallest displacement was in the inferior wall ( $0.73 \pm 1.67$  mm). Interfraction: Table 2 shows that bladder wall displacement was greatest in the anterior wall [9.04 (11.13) mm,

5.71 (23.86) mm], followed by the superior wall [5.87 (12.33) mm, -3.14 (23.60) mm].

### Displacement of the target volume and OARs

#### Intrafraction

In Fig. 3 (a-c) and Supplementary Tables 2 and 3, the range of motion of the CTV along the XYZ axis is within 5 mm, and the range of motion along the Z axis is larger than that along the YZ axis (-4.68 to 4.78 mm). The bladder exhibits motion along the Z axis with a range of -2 to 13.68 mm, predominantly in the superior direction, with an average displacement of  $4.14 \pm 3.87$  mm. The rectum shows motion along the X axis within the range of -5 to 5 mm, while the upper rectum demonstrates significant motion along the Z axis within the range of -13.51 to 15.66 mm, with average displacements of 4.74 mm and 5.94 mm in the cranial and caudal directions, respectively. The middle rectum displays substantial motion along the Y axis (-11.47 to 9.67), with average displacements of 4.33 mm and 3.88 mm in the anterior and posterior directions, respectively. The range of motion of the CTV along the XYZ axis is within 5 mm, and the range of motion along the Z axis is larger than that along the YZ axis (-4.68 to 4.78) mm.

#### Interfraction

In Fig. 3 (e, f) and Supplementary Tables 2 and 3, the CTV has a range of motion of 5 mm along the X axis and maximum distances of 7.45 mm along the Y axis and 6.59 mm along the Z axis. Compared to CT, the pre-MR images showed that the bladder had a larger motion range along the YZ axes, with mean displacements of -3.84 mm and 3.54 mm, respectively. The upper ( $8.04 \pm 11.62$  mm) and lower ( $6.19 \pm 11.16$  mm) rectum exhibited the greatest motion along the Z axis. The middle rectum had the greatest motion along the Y axis ( $6.60 \pm 8.02$  mm). In Fig. 3 (h, i), compared to CT images, the post-MR images showed minimal differences in bladder volume (20.3 ml), indicating less noticeable motion. The motion of the upper, middle, and lower rectum was mainly concentrated along the YZ axes.

### Motion correlation analysis

#### Intrafraction

As shown in Fig. 4, there was a positive correlation between the bladder volume increment ( $\Delta v$ ) and the displacement of the bladder superior wall and the displacement of the bladder centroid Z axis (Cr-C) ( $r=0.74$ ,  $r=0.73$ ,  $P<0.05$ ), and there was also a significant correlation between the latter two variables ( $r=0.93$ ,  $P<0.05$ ).  $\Delta v$  was moderately positively correlated with the displacement of the bladder anterior wall and left wall ( $r=0.62$ ,  $r=0.65$ ,  $P<0.05$ ). The displacement of the bladder anterior wall was negatively correlated with the

displacement of the bladder centroid Y axis (A-P) and showed a strong correlation ( $r=-0.72$ ,  $P<0.05$ ). Furthermore, the displacement of the bladder posterior wall was moderately correlated with the displacement of the whole rectum and the lower segment of the rectum centroid Y axis (A-P) ( $r=0.63$ ,  $r=0.62$ ,  $P<0.05$ ). The correlation between  $\Delta v$  and the displacement of the CTV and PTV centroids was weak ( $r<0.2$ ), while the displacement of the bladder posterior wall was correlated with the displacement of the CTV centroid Y axis (A-P) ( $r=0.50$ ,  $P<0.05$ ).

### Dosimetric differences

#### Interfraction

The dose-volume histogram (DVH) parameters of the PTV are detailed in Table 3. Statistically significant differences were found for D50, D98, Dmean, and Dmin. Compared to those in the CT plan, D98 (7.5 Gy, 7.54 Gy) and Dmin (15.94, 15.40 Gy) decreased significantly, while Dmean decreased slightly. Table 4 shows the detailed values of the OAR parameters, with statistically significant differences in rectal volume, V10, V30, V35, V40, Dmean, and Dmax compared to those of the CT plan, and the Dmean and Dmin of the spinal cord also showed statistically significant differences. **Intrafraction:** There were only minor differences in DVH parameters for either the target volume or the OARs, and they were not statistically significant.

### Discussion

Accurate target localization is crucial for treating cervical cancer [33]. Uncertainties arise from both inter- and intrafractional motion, with interfractional motion potentially having a greater impact [34]. Interfractional motion may result from the movement and deformation of a tumor and the surrounding organ and changes in volume. Therefore, applying margins to the CTV in a rational manner is essential to achieve high precision [34].

In this study, we found that the CTV intrafractional motion range was within 5 mm along the XYZ axis. This result is similar to the findings of Visser J et al. [35] who also concluded that an online MRI-guided strategy with a 5 mm PTV margin for the CTV of cervix-uterus is sufficient to account for intrafraction anatomical changes. However, the study did not use Unity for treatment and only administered weekly MRIs, not truly MR-guided online adaptive radiotherapy. In contrast, our experimental results are more credible. We believe that the 5 mm isotropic PTV margins are well suited for the ATS workflow of the 1.5T MR-Linac. This is because the ATS process generates a plan based on the new anatomy prior to each treatment [17, 23, 36], so it is only necessary to consider intrafraction motion. For interfraction motion,

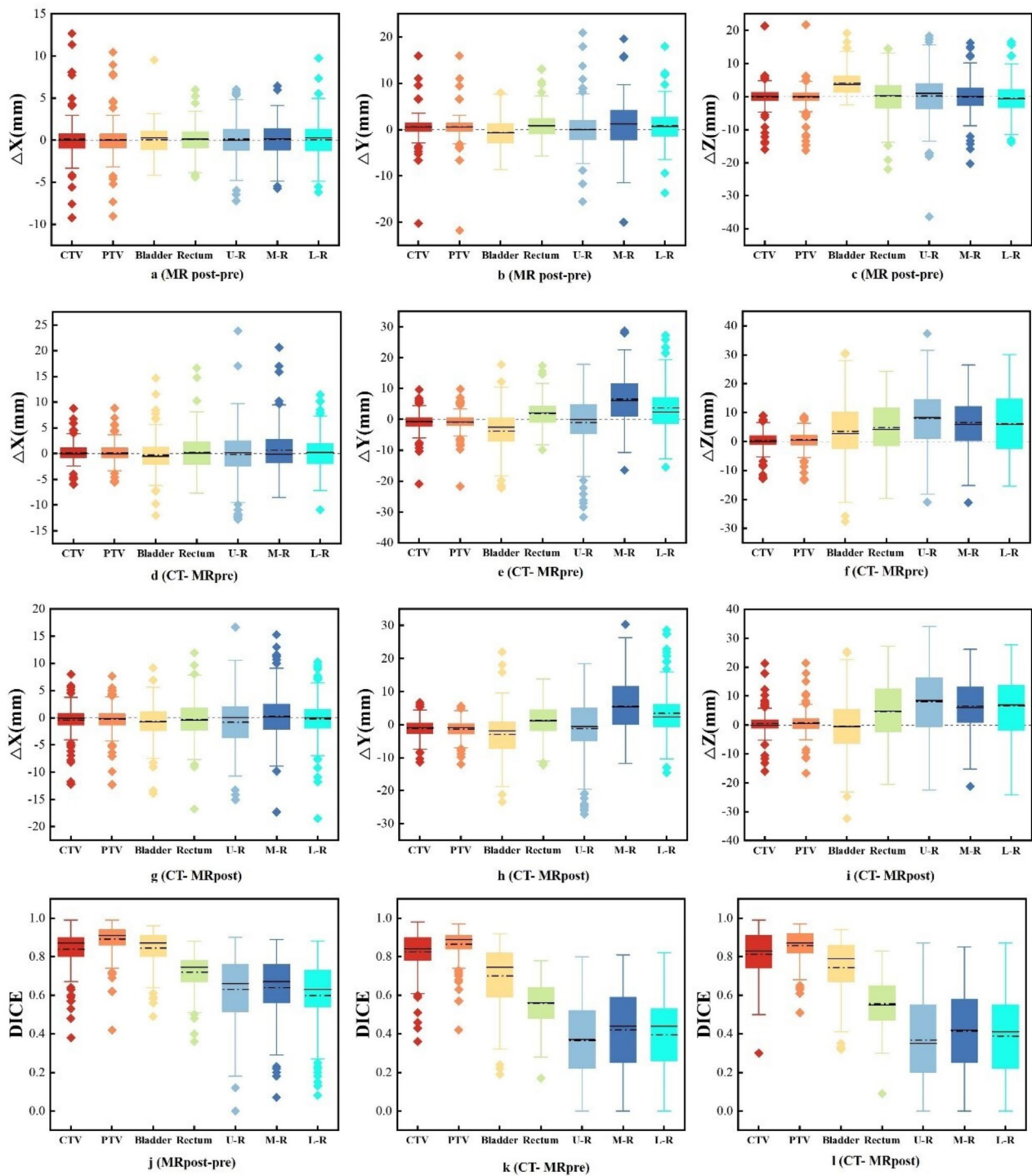


**Fig. 3** a-c shows the intrafractional motion along the XYZ axis, d-i show the interfractional motion along the XYZ axis, and j-l show the DICE coefficient. Right, cranial, and anterior movements have positive values, while movements in the opposite direction have negative values. U-R, upper rectum; M-R, middle rectum; and L-R, lower rectum. In the box plot, the solid line represents the median, and the dashed line represents the mean

the CTV has a range of motion of 5 mm along the X axis and maximum distances of 7.45 mm along the Y axis and 6.59 mm along the Z axis. Therefore, isotropic 5 mm PTV margins do not provide enough coverage, and anisotropic margins are needed. This conclusion was laterally verified

by the findings of Tachiki et al. [37], who reported that the mean displacements of the COM was 3.7 mm (anterior), 6.80 mm (posterior), 3.29 mm (superior), 7.01 mm (inferior), 1.66 mm (left), and 2.93 mm (right). Therefore, we recommend anisotropic PTV margins of 5 mm in the

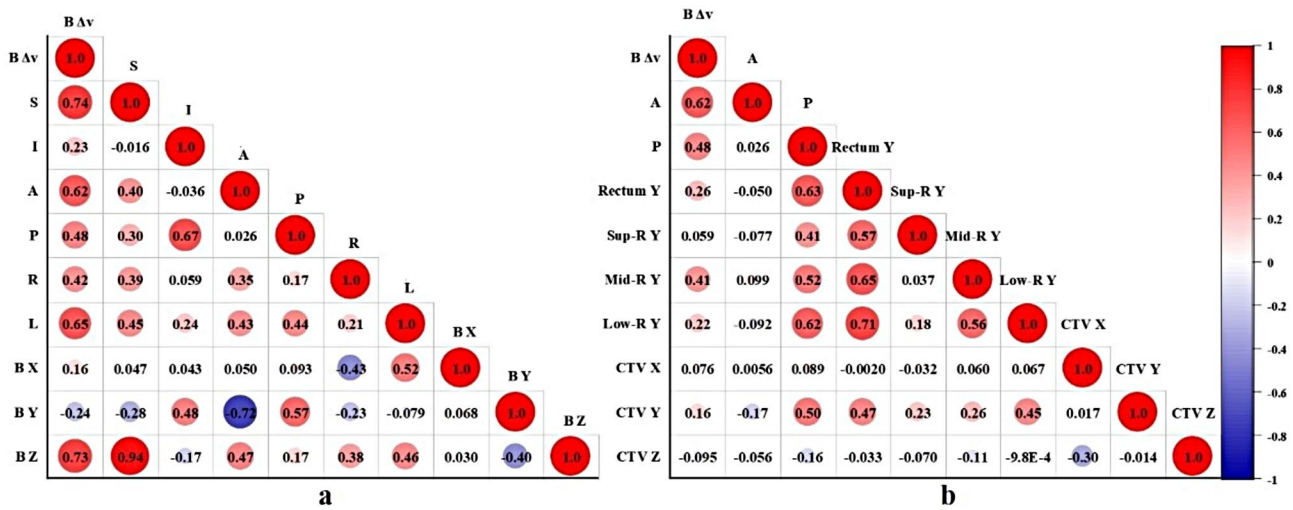


**Fig. 4** Correlation analysis plot. Red indicates a positive correlation, while blue indicates a negative correlation. The range of correlation coefficient (R) values is -1 to 1, where a larger |R| indicates a stronger correlation. S-I, superior-inferior; A-P, anterior-posterior; and R-L, right-left. B, bladder;  $\Delta$ v, bladder volume increment. Sup-R, super rectum; Mid-R, middle rectum; and Low-R, lower rectum

**Table 3** Dose-volume parameters of the PTV

Parameters	PlanA	PlanA1	PlanA2	ANOVA P value	P value		
					PlanA vs. PlanA1	PlanA vs. PlanA2	PlanA1 vs. PlanA2
Volume (ml)	849.27 ± 235.99	903.58 ± 244.91	912.34 ± 255.86	0.339	0.473	0.491	1.000
D1 cc (Gy)	59.99 ± 1.54	59.66 ± 1.55	58.06 ± 1.57	0.425	0.637	0.637	1.000
D2 (Gy)	58.06 ± 1.19	57.77 ± 1.15	57.77 ± 1.18	0.368	0.562	0.507	1.000
D50 (Gy)	53.56 ± 0.38	53.21 ± 0.42	53.17 ± 0.51	0.000*	0.000*	0.000*	1.000
D98 (Gy)	48.54 ± 6.47	41.04 ± 10.74	41.00 ± 11.01	0.000*	0.000*	0.000*	1.000
Dmean (Gy)	53.62 ± 0.50	52.63 ± 1.01	52.65 ± 1.19	0.000*	0.000*	0.000*	1.000
Dmax (Gy)	61.65 ± 1.75	60.93 ± 1.72	60.92 ± 1.76	0.098	0.134	0.108	1.000
Dmin (Gy)	34.98 ± 13.39	19.04 ± 13.55	19.58 ± 13.90	0.000*	0.000*	0.000*	1.000
HI	1.22 ± 0.07	1.20 ± 0.06	1.20 ± 0.07	0.073	0.094	0.081	1.000
CI	1.12 ± 0.30	1.05 ± 0.35	1.03 ± 0.31	0.919	1.000	1.000	1.000

PlanA, CT plan; PlanA1, Mapping the planA dose distribution to the pre-MR image. PlanA2, Mapping the planA dose distribution to the post-MR image. Dx represents the dose received by X% of the target volume; Dmax, maximum dose; Dmean, mean dose; Dmin, minimum dose; HI, heterogeneity index; and CI, conformity index. \* represents a statistically significant difference

R/L direction, 8 mm in the A/P direction, and 7 mm in the Cr/C direction. It is also recommended that an anisotropic PTV margin be used in the ATP workflow. This is because the ATP workflow only considers changes in position and does not consider the deformation of anatomical structures [23], so a larger PTV margin is needed.

The bladder and the UCC target volume are anatomically closely linked, and changes in bladder filling have a profound influence on the shape and position of the cervix and uterus [33, 38]. Although many studies have explored the effect of bladder volume changes on the movement of the UCC target volume, few studies have discussed the relationship between bladder wall changes and the motion of the UCC target volume [39–41]. Our findings showed that bladder wall displacement within the intrafraction was greatest in the superior wall (9.30 ± 8.77 mm), followed by

the anterior wall (3.28 ± 4.89 mm) and least in the inferior wall (0.73 ± 1.67 mm). The motion was mainly centered on the superior and anterior sides. In comparison, the posterior wall displacement (2.66 ± 4.44 mm) was not significant, but the displacement of the bladder posterior wall was correlated with the displacement of the CTV centroid Y axis (A–P) ( $r=0.50$ ,  $P<0.05$ ). The findings of Kerkhof EM et al. [39] and Nagao A et al. [40] laterally confirmed that there was a correlation between bladder filling and CTV movement in patients with UCC ( $r=0.46$ ,  $P<0.01$ ;  $r=0.61$ ,  $P<0.01$ ), but these two studies did not explore the correlation between the bladder wall and CTV movement. In the future, we will design experiments to explore the effect of different bladder filling methods (emptying or filling) on CTV displacement to refine our study and choose the appropriate filling methods. In addition, bladder filling also affects rectal motion.

**Table 4** Dose–volume parameters of the OARs

Parameters	PlanA	PlanA1	PlanA2	ANOVA P value	P value		
					PlanA vs. PlanA1	PlanA vs. PlanA2	PlanA1 vs. PlanA2
<b>Bladder</b>							
Volume (ml)	426.50 ± 189.06	320.18 ± 144.12	406.20 ± 174.14	0.000*	0.010*	1.000	0.000*
V20	96.21 ± 2.80	96.99 ± 2.22	96.85 ± 2.23	0.365	0.484	0.921	1.000
V30	65.68 ± 6.76	67.69 ± 8.21	67.60 ± 7.69	0.348	0.440	0.748	1.000
V40	36.01 ± 8.15	38.98 ± 10.43	39.06 ± 10.06	0.180	0.207	0.274	1.000
V50	9.71 ± 5.40	11.91 ± 7.92	12.84 ± 8.35	0.146	0.589	0.172	0.918
Dmean (Gy)	35.64 ± 1.90	36.41 ± 2.42	36.48 ± 2.41	0.203	0.268	0.262	1.000
Dmax (Gy)	56.21 ± 1.68	55.88 ± 2.15	56.29 ± 2.09	0.129	0.399	1.000	0.246
Dmin (Gy)	14.47 ± 3.5	15.64 ± 3.29	15.36 ± 3.37	0.105	0.104	0.322	1.000
<b>Rectum</b>							
Volume (ml)	58.20 ± 23.51	43.31 ± 16.42	43.44 ± 17.40	0.001*	0.002*	0.000*	1.000
V10	95.98 ± 6.93	96.68 ± 4.72	97.01 ± 4.57	0.000*	0.000*	0.000*	1.000
V20	92.11 ± 9.19	91.56 ± 7.66	92.21 ± 7.16	0.046	0.040	0.103	1.000
V30	83.50 ± 14.51	80.55 ± 15.455	81.35 ± 14.69	0.000*	0.000*	0.000*	1.000
V35	74.77 ± 17.83	71.74 ± 20.48	72.455 ± 19.68	0.000*	0.000*	0.000*	1.000
V40	59.74 ± 21.21	57.34 ± 24.93	58.02 ± 24.40	0.000*	0.000*	0.000*	1.000
V50	14.36 ± 11.14	14.28 ± 13.44	14.65 ± 13.69	0.617	1.000	0.983	1.000
Dmean (Gy)	39.58 ± 55.05	39.04 ± 0.555	39.30 ± 5.31	0.000*	0.000*	0.000*	1.000
Dmax (Gy)	54.97 ± 2.055	53.99 ± 2.76	54.03 ± 2.47	0.005*	0.103	0.005*	0.257
Dmin (Gy)	13.71 ± 9.62	11.46 ± 7.80	11.89 ± 7.93	0.224	0.266	0.656	1.000
<b>Spinal-cord</b>							
Dmean (Gy)	5.44 ± 2.82	12.28 ± 6.83	13.02 ± 7.64	0.000*	0.000*	0.000*	1.000
Dmax (Gy)	34.39 ± 11.11	34.17 ± 11.24	34.47 ± 10.94	0.998	1.000	1.000	1.000
Dmin (Gy)	0.25 ± 0.22	1.32 ± 0.87	1.57 ± 1.80	0.000*	0.000*	0.000*	1.000

PlanA, CT plan; PlanA1, Mapping the planA dose distribution to the pre-MR image. PlanA2, Mapping the planA dose distribution to the post-MR image. Dx represents the dose received by X% of the target volume; Dmax, maximum dose; Dmean, mean dose; Dmin, minimum dose; HI, heterogeneity index; and CI, conformity index. \* represents a statistically significant difference

A correlation was found between posterior bladder wall displacement and motion along the Y axis (A–P) for the whole rectum centroid ( $r=0.63$ ,  $P<0.05$ ), with the strongest correlation in the lower rectum ( $r=0.62$ ,  $P<0.05$ ), followed by the middle ( $r=0.52$ ,  $P<0.05$ ) and the upper ( $r=0.41$ ,  $P<0.05$ ) rectum. We did not find a correlation between changes in rectal volume and UCC CTV movements; however, Tyagi N et al. [41] found that a 10-cc increase in rectal volume corresponds to a superior shift in the CTV centroid position of 0.25 mm and a posterior shift of 0.52 mm. This may be related to the different approaches used for rectal emptying management. Nevertheless, we found a weak correlation between the rectum and the shift along the CTV centroid Y axis (A–P) shift ( $r=0.47$ ,  $P<0.05$ ).

UCC is a disease for which ART is typically appropriate and necessary. It has been noted in the practice of radiation therapy for patients with UCC that intra- and interfraction displacement and deformation of the pericervical OARs negatively affect the delivery of the planned dose, which has the potential to decrease the rate of local tumor control or increase normal tissue toxicity [42]. In our study, the original PlanA dose distribution

was directly mapped to MR images with contours to form PlanA1 and PlanA2, and then, the actual doses received by the PTV and OARs were analyzed, which revealed undercoverage of the target volume for the prescribed dose and a significant decrease in D98 (7.5 Gy, 7.54 Gy). In a study using fan beam CT-guided external ART for patients with UCC, Peng et al. [43] used a study method similar to ours to directly map the dose distribution of the original Plan0 to the adaptive target volume to form VPlan. The target volume coverage of the prescribed dose was insufficient, and the rectal Dmax and V40 were greater than the prescribed dose. In addition, dose optimization calculations based on the new anatomy were performed to obtain Aplan, whose dosimetric parameters almost all met the criteria. The results of their study demonstrated that online ART in external RT for UCC significantly improved the dose distribution and could become an ideal technology for achieving individualized precise RT. The uRT-Linac (United Imaging Healthcare Co., Ltd., Shanghai, China) method used in their study has a function similar to that of Unity, but the latter has the advantages of acquiring guided images without radiation as well as superior soft tissue resolution. In addition,

the dosimetric accuracy and advantages of using MR-Linac for the ART of other tumors in the abdominopelvic region, e.g., prostate cancer [44, 45], rectal cancer [46, 47], and pancreatic cancer [48], have been demonstrated while decreasing gastrointestinal and genitourinary toxicity [49, 50].

There are several limitations in our study. First, there are some errors in the image fusion alignment of the two modalities, CT and MR, which can affect the accuracy of motion assessment. Second, we considered a small sample size of 32 patients. Finally, the use of centroid displacement to assess the motion of the target volume and OARs may not be the best approach, and the placement of metallic markers may be more effective but can be invasive for the patient. Although our study revealed the use of MR-Linac-guided ART for UCC, significant motion of OARs, such as the bladder and rectum, was also observed and will be further explored in the future for other tumors in the abdominopelvic region, such as bladder cancer and rectal cancer.

## Conclusion

During ART for patients with UCC using MR-Linac, significant motion of the CTV can be observed. Therefore, we recommend the use of an ATS workflow with an isotropic PTV margin of 5 mm based on intrafraction motion. Based on interfraction motion, the recommended ATP workflow uses anisotropic PTV margins of 5 mm in the R/L direction, 8 mm in the A/P direction, and 7 mm in the Cr/C direction. Interfractional motion resulted in a significant decrease in the target volume dose below the prescribed level. Therefore, there is a great need to use MR-Linac and generate new adaptive treatment plans for patients based on the new anatomy and appropriate PTV margins to compensate for dosimetric errors due to motion.

## Abbreviations

UCC	uterine cervical cancer
ART	adaptive radiotherapy
DVH	dose–volume histogram
L–R	left–right
A–P	anterior–posterior
Cr–C	cranial–caudal
EBRT	external beam radiotherapy
IMRT	intensity-modulated radiotherapy
3D-CRT	three-dimensional conformal radiotherapy
MRI	Magnetic resonance imaging
MRgRT	MR-guided radiation therapy
CTV	clinical target volume
GTV	gross tumor volume
CTV	clinical tumor volume
PTV	planning target volume
OAR	organs at risk
CBCT	cone-beam computed tomography
FIGO	Federation International of Gynecology and Obstetrics
RTOG	Radiation Therapy Oncology Group
GPUMCD	GPU-based Monte Carlo dose calculation platform
SD	standard deviation

## Supplementary Information

The online version contains supplementary material available at <https://doi.org/10.1186/s13014-024-02569-5>.

Supplementary Material 1

## Acknowledgements

The authors would like to thank all the members for their thoughtful suggestions and comments on the manuscript and all the sources of financial support.

## Author contributions

Conceived and designed the analysis: HDW, ZJL; Collected the data: HDW, ZKL, DXS, PJY, BZL, JMZ, QQT, MWC; Performed the analysis: HDW; Wrote the paper: HDW; Critical review: ZJL; Supervision: YY. All authors read and approved the final manuscript.

## Funding

This study was supported by the National Natural Science Foundation of China (Grant No. 82102173/82072094/12475343) and the Taishan Scholars Young Experts Fund (Grant NO.tsqn202408375).

## Data availability

No datasets were generated or analysed during the current study.

## Declarations

### Ethics approval and consent to participate

This study was reviewed and approved by the Institutional Review Board of Shandong Cancer Hospital. All methods used in this study were carried out in accordance with relevant guidelines and regulations. Informed consent to participate in the study was obtained from all study participants for personally identifiable data.

### Consent for publication

Not applicable.

### Competing interests

The authors declare no competing interests.

### Author details

<sup>1</sup>Department of Radiation Oncology Physics and Technology, Shandong Cancer Hospital and Institute, Shandong First Medical University and Shandong Academy of Medical Sciences, Jinan, China

<sup>2</sup>Department of Graduate Science, Shandong First Medical University (Shandong Academy of Medical Sciences), Jinan, China

<sup>3</sup>Chengdu University of Technology, Chengdu, China

<sup>4</sup>Nanjing University of Aeronautics and Astronautics, Nanjing, China

<sup>5</sup>Southeastern University, Nanjing, China

Received: 4 January 2024 / Accepted: 6 December 2024

Published online: 18 December 2024

## References

1. Sung H, Ferlay J, Siegel RL, et al. Global Cancer statistics 2020: GLOBOCAN estimates of incidence and Mortality Worldwide for 36 cancers in 185 countries. *CA Cancer J Clin.* 2021;71(3):209–49.
2. Siegel RL, Miller KD, Fuchs HE et al. Cancer statistics, 2022. *CA Cancer J Clin* 2022, 72(1).
3. Tan Mbbs Mrpc Frmr Md Lt, Tanderup PhD K, Kirisits PhD C, et al. Image-guided adaptive Radiotherapy in Cervical Cancer. *Semin Radiat Oncol.* 2019;29(3):284–98.
4. Cohen PA, Jhingran A, Oaknin A, et al. Cervical cancer. *Lancet (London England).* 2019;393(10167):169–82.
5. Masui T, Sato A, Nakano K, et al. The advantage of the Intensity Modulated Radiation Therapy (IMRT) comparing to the conventional radiation therapy in neoadjuvant settings. *Pancreatol.* 2016;16(4):S168.

6. Weiss Y, Chin L, Younus E, et al. Cine MRI-based analysis of intrafractional motion in radiation treatment planning of head and neck cancer patients. *Radiation Oncology: J Eur Soc Therapeutic Radiol Oncol*. 2023;186:109790.
7. Chuter RW, Brewster F, Retout L et al. Feasibility of using a dual isocentre technique for treating cervical cancer on the 1.5 T MR-Linac. *Phys Med Biol* 2023, 68(2).
8. Ríos I, Vázquez I, Cuervo E, et al. Problems and solutions in IGRT for cervical cancer. *Rep Pract Oncol Radiother*. 2018;23(6):517–27.
9. Rigaud B, Simon A, Gobeli M, et al. CBCT-guided evolutive library for cervical adaptive IMRT. *Med Phys*. 2018;45(4):1379–90.
10. Maemoto H, Toita T, Ariga T, et al. Predictive factors of uterine movement during definitive radiotherapy for cervical cancer. *J Radiat Res (Tokyo)*. 2017;58(3):397–404.
11. Ding GX, Munro P, Pawlowski J, et al. Reducing radiation exposure to patients from KV-CBCT imaging. *Radiation Oncology: J Eur Soc Therapeutic Radiol Oncol*. 2010;97(3):585–92.
12. Chen L, Liang X, Shen C et al. Synthetic CT generation from CBCT images via unsupervised deep learning. *Phys Med Biol* 2021, 66(11).
13. Wang H, Liu X, Kong L, et al. Improving CBCT image quality to the CT level using RegGAN in esophageal cancer adaptive radiotherapy. *Strahlenther Onkol*. 2023;199(5):485–97.
14. Li Z, Zhang Q, Li H, et al. Using RegGAN to generate synthetic CT images from CBCT images acquired with different linear accelerators. *BMC Cancer*. 2023;23(1):828.
15. Chang Y, Liang Y, Yang B, et al. Dosimetric comparison of deformable image registration and synthetic CT generation based on CBCT images for organs at risk in cervical cancer radiotherapy. *Radiation Oncol (London England)*. 2023;18(1):3.
16. Suwanraksa C, Bridhikitti J, Liamsuwan T et al. CBCT-to-CT translation using Registration-based generative adversarial networks in patients with Head and Neck Cancer. *Cancers (Basel)* 2023, 15(7).
17. Dassen MG, Janssen T, Kusters M, et al. Comparing adaptation strategies in MRI-guided online adaptive radiotherapy for prostate cancer: implications for treatment margins. *Radiation Oncology: J Eur Soc Therapeutic Radiol Oncol*. 2023;186:109761.
18. Randall JW, Rammohan N, Das IJ et al. Towards Accurate and Precise Image-Guided Radiotherapy: Clinical Applications of the MR-Linac. *Journal of clinical medicine* 2022, 11(14).
19. Fast M, van de Schoot A, van de Lindt T, et al. Tumor Trailing for Liver SBRT on the MR-Linac. *Int J Radiat Oncol Biol Phys*. 2019;103(2):468–78.
20. Berger T, Seppenwoolde Y, Pötter R, et al. Importance of technique, Target Selection, Contouring, dose prescription, and dose-planning in External Beam Radiation Therapy for Cervical Cancer: evolution of practice from EMBRACE-1 to II. *Int J Radiat Oncol Biol Phys*. 2019;104(4):885–94.
21. Raaymakers BW, Lagendijk JJ, Overweg J, et al. Integrating a 1.5 T MRI scanner with a 6 MV accelerator: proof of concept. *Phys Med Biol*. 2009;54(12):N229–237.
22. Lagendijk JJ, Raaymakers BW, van Vulpen M. The magnetic resonance imaging-linac system. *Semin Radiat Oncol*. 2014;24(3):207–9.
23. Winkel D, Bol GH, Kroon PS, et al. Adaptive radiotherapy: the Elekta Unity MR-linac concept. *Clin Translational Radiation Oncol*. 2019;18:54–9.
24. Wang H, Liu X, Song Y, et al. Feasibility study of adaptive radiotherapy for esophageal cancer using artificial intelligence autosegmentation based on MR-Linac. *Front Oncol*. 2023;13:1172135.
25. Langerak TR, Mens JWM, Quint S, et al. PD-0552: cervix motion in 50 cervical cancer patients, derived from daily CBCT and implanted fiducials. *Radiation Oncol*. 2014;111(1):S216.
26. Taylor A, Powell ME. Conformal and intensity-modulated radiotherapy for cervical cancer. *Clin Oncol (R Coll Radiol)*. 2008;20(6):417–25.
27. Berger T, Godart J, Jagt T, et al. Dosimetric Impact of Intrafraction Motion in Online-Adaptive Intensity Modulated Proton Therapy for Cervical Cancer. *Int J Radiat Oncol Biol Phys*. 2021;109(5):1580–7.
28. Visser J, de Boer P, Crama KF, et al. Dosimetric comparison of library of plans and online MRI-guided radiotherapy of cervical cancer in the presence of intrafraction anatomical changes. *Radiation Oncol (London England)*. 2019;14(1):126.
29. Eminowicz G, Rompokos V, Stacey C, et al. Understanding the impact of pelvic organ motion on dose delivered to target volumes during IMRT for cervical cancer. *Radiation Oncology: J Eur Soc Therapeutic Radiol Oncol*. 2017;122(1):116–21.
30. Li X, Wang L, Cui Z, et al. Online MR evaluation of inter- and intra-fraction uterus motions and bladder volume changes during cervical cancer external beam radiotherapy. *Radiation Oncol (London England)*. 2021;16(1):179.
31. Bhatla N, Aoki D, Sharma DN, et al. Cancer of the cervix uteri: 2021 update. *Int J Gynaecol Obstet*. 2021;155(Suppl 1):28–44.
32. Small W, Bosch WR, Harkenrider MM, et al. NRG Oncology/RTOG Consensus guidelines for Delineation of Clinical Target volume for Intensity modulated Pelvic Radiation Therapy in Postoperative Treatment of Endometrial and Cervical Cancer: an update. *Int J Radiat Oncol Biol Phys*. 2021;109(2):413–24.
33. Zeng Z, Zhu J, Wang Z, et al. Pelvic target volume inter-fractional motion during radiotherapy for cervical cancer with daily iterative cone beam computed tomography. *Radiation Oncol (London England)*. 2024;19(1):48.
34. Chan P, Dinniwell R, Haider MA, et al. Inter- and intrafractional tumor and organ movement in patients with cervical cancer undergoing radiotherapy: a cinematic-MRI point-of-interest study. *Int J Radiat Oncol Biol Phys*. 2008;70(5):1507–15.
35. Visser J, de Boer P, Crama KF, et al. Dosimetric comparison of library of plans and online MRI-guided radiotherapy of cervical cancer in the presence of intrafraction anatomical changes. *Radiat Oncol*. 2019;14(1):126.
36. Lee D, Renz P, Oh S et al. Online adaptive MRI-Guided stereotactic body radiotherapy for pancreatic and other Intra-abdominal Cancers. *Cancers (Basel)* 2023, 15(21).
37. Tachiki L, Chen J, Hsu IC, et al. Quantification of interfractional uterus motion for intact cervical cancer patients. *Gynecol Oncol*. 2014;135(2):403.
38. Bondar L, Hoogeman M, Mens JW, et al. Toward an individualized target motion management for IMRT of cervical cancer based on model-predicted cervix-uterus shape and position. *Radiation Oncology: J Eur Soc Therapeutic Radiol Oncol*. 2011;99(2):240–5.
39. Kerkhof EM, van der Put RW, Raaymakers BW, et al. Intrafraction motion in patients with cervical cancer: the benefit of soft tissue registration using MRI. *Radiation Oncology: J Eur Soc Therapeutic Radiol Oncol*. 2009;93(1):115–21.
40. Nagao A, Okamoto H, Nakayama H, et al. Assessment of intrafractional motion of the cervix-uterus by MR-guided radiotherapy system†. *J Radiat Res*. 2023;64(6):967–72.
41. Tyagi N, Lewis JH, Yashar CM, et al. Daily online cone beam computed tomography to assess interfractional motion in patients with intact cervical cancer. *Int J Radiat Oncol Biol Phys*. 2011;80(1):273–80.
42. Tanderup K, Georg D, Pötter R, et al. Adaptive management of cervical cancer radiotherapy. *Semin Radiat Oncol*. 2010;20(2):121–9.
43. Peng H, Zhang J, Xu N, et al. Fan beam CT-guided online adaptive external radiotherapy of uterine cervical cancer: a dosimetric evaluation. *BMC Cancer*. 2023;23(1):588.
44. Brennan VS, Burlison S, Kostrzewa C, et al. SBRT focal dose intensification using an MR-Linac adaptive planning for intermediate-risk prostate cancer: an analysis of the dosimetric impact of intra-fractional organ changes. *Radiation Oncology: J Eur Soc Therapeutic Radiol Oncol*. 2023;179:109441.
45. Xiong Y, Rabe M, Nierer L, et al. Assessment of intrafractional prostate motion and its dosimetric impact in MRI-guided online adaptive radiotherapy with gating. *Strahlenther Onkol*. 2023;199(6):544–53.
46. Eijkelenkamp H, Boekhoff MR, Verweij ME, et al. Planning target volume margin assessment for online adaptive MR-guided dose-escalation in rectal cancer on a 1.5 T MR-Linac. *Radiation Oncology: J Eur Soc Therapeutic Radiol Oncol*. 2021;162:150–5.
47. Feng X, Tang B, Yao X, et al. Effectiveness of bladder filling control during online MR-guided adaptive radiotherapy for rectal cancer. *Radiation Oncol (London England)*. 2023;18(1):136.
48. Koay EJ, Hanania AN, Hall WA, et al. Dose-escalated Radiation Therapy for Pancreatic Cancer: a simultaneous Integrated Boost Approach. *Pract Radiat Oncol*. 2020;10(6):e495–507.
49. Eijkelenkamp H, Grimbergen G, Daamen LA, et al. Clinical outcomes after online adaptive MR-guided stereotactic body radiotherapy for pancreatic tumors on a 1.5 T MR-linac. *Front Oncol*. 2023;13:1040673.
50. Nicosia L, Mazzola R, Rigo M, et al. Linac-based versus MR-guided SBRT for localized prostate cancer: a comparative evaluation of acute tolerability. *Radiol Med*. 2023;128(5):612–8.

## Publisher's note

Springer Nature remains neutral with regard to jurisdictional claims in published maps and institutional affiliations.